


Combined Electrospray-Scanning Mobility Particle Sizer (ES-SMPS) and Time-Resolved Synchrotron Radiation-Small-Angle X-ray Scattering (SR-SAXS) Investigation of Colloidal Silica Aggregation. Part II. Influence of Aggregation Initiator on Gel Stability

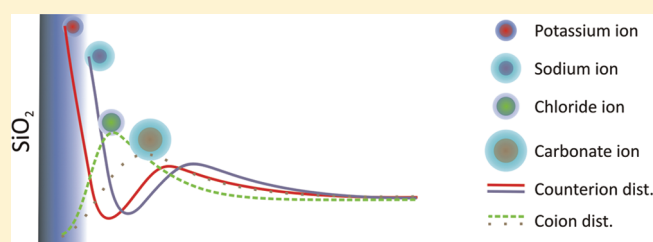
Ann-Cathrin J. H. Johnsson,^{*,†} M. Caterina Camerani,[‡] and Zareen Abbas[†]

[†]Department of Chemistry, University of Gothenburg, Gothenburg, Sweden

[‡]Eka Chemicals AB, AkzoNobel, Bohus, Sweden

 Supporting Information

ABSTRACT: The effect of ion specificity on the slow aggregation of silica nanoparticles with various initial morphology was investigated with an electrospray-scanning mobility particle sizer (ES-SMPS) and time-resolved synchrotron radiation-small-angle X-ray scattering (SR-SAXS). This combination provides a unique tool to monitor and resolve the early aggregate development in detail. Aggregation was induced by varying the K_2CO_3 or KCl concentration to obtain a fixed gelation time of ~ 40 min, and the results were compared with those obtained in a previous paper (Johnsson et al. *J. Phys. Chem. B* **2011**, *115*, 765–775) for NaCl. All dispersions produced gels that contained free primary particles well past the point of gelation (PoG). The initial aggregate formation and obtained gel morphologies were independent of the aggregation initiator. Nevertheless, ion-specific effects were observed for the rate of the stability increase of the 3-dimensional (3D) gel structure. The formation of a stable structure was fastest in the presence of the strongly hydrated counterions, and a clear anion effect was observed. The obtained gel stabilities were interpreted by relating the rate of formation of covalent siloxane bonds to the polarization of the water molecules surrounding structure-maker ions.



1. INTRODUCTION

In a previous paper the effect of initial particle morphology on the aggregation behavior and morphology of the solid gels produced was investigated.¹ It was found that the initial morphology had a profound effect on the early stages of aggregate formation which in turn affected the morphology and stability of the formed gels. The initial aggregate formation can be influenced by changes in pH or the bulk electrolyte concentration,^{2,3} or by addition of polymers.⁴ In addition, the interactions can be influenced by the nature of the ionic species; ions of equal charge and concentration affect the aggregation of the silica particles differently, an effect known as ion specificity.^{5,6} Here we present the effect of aggregation initiator on the morphology and strength increase of the solid silica gel.

Ion specificity was first discovered by Hofmeister, who ordered electrolytes in a sequence according to their efficiency to salt-out egg white.⁶ The ions adsorb according to the direct Hofmeister sequence if the surface affinity increases with increasing bare ion radius ($Li^+ < Na^+ < K^+ < Rb^+ < Cs^+$), whereas the indirect sequence refers to Li^+ ions being preferentially adsorbed compared to Cs^+ ions.⁶ It has been shown that the observed adsorption sequence, that is, whether it is direct or indirect at a specific surface, depends on the nature of that surface.⁷ Generally, the direct sequence is observed for oxides with low

isoelectric point (IEP), and the indirect sequence is observed for high IEP oxides.⁶ In fact, for particles of the same substance, synthesized to yield different IEPs, a clear reversal of the adsorption sequence was observed when going from low to high IEP surfaces.⁸ The IEP of silica is around pH 2, and the surface affinity of the counterions has been shown to increase with increasing unhydrated radii, that is, according to the direct sequence.^{7,9,10} The most apparent effect of ion specificity on colloidal aggregation is the decrease of the critical coagulation concentration (CCC) due to the increased adsorption.^{7,11} Furthermore, ion-specific surface interactions affect the distribution of ions near the surface,¹² and ions adsorbed at the particle surfaces can interact in a van der Waals “like” interaction. This attractive interaction originates from local polarization of the ion layers due to charge fluctuations, and it is known as the electrostatic ion–ion correlation (IIC) interaction.^{13,14} In monovalent systems the effect of the IIC attraction is noticeable only for strongly adsorbed ions.¹³ It has been suggested this additional attraction can influence the microstructure and strength of the silica gel network,^{10,15,16} and this could lead to a more stable gel structures.^{10,16}

Received: April 8, 2011

Revised: June 8, 2011

Published: July 20, 2011

Table 1. Electrolyte Concentrations and wt % SiO₂ in the K₂CO₃ and KCl Aggregation Mixtures and the Obtained Points of Gelation (PoG)

electrolyte sample	K ₂ CO ₃			KCl		
	conc. K ⁺ (M)	SiO ₂ (wt %)	PoG (min)	conc. K ⁺ (M)	SiO ₂ (wt %)	PoG (min)
Sol 1	0.339	34.6	39	0.221	36.1	41
Sol 2	0.408	32.4	40	0.258	34.5	41
Sol 3 Dec	0.285	12.4	42	0.182	13.1	43
Sol 3 July	0.334	12.0	38	0.202	12.9	37

The ion adsorption at the silica surface has been related to the hydrated structures of both the surface and the counterions.^{5,8,11} An ion that promotes a water structure is categorized as a structure maker, while ions that disrupt the water structure in their vicinity are known as structure breakers.¹⁷ Likewise, particle surfaces can promote or disrupt water structures, and these are known as structure-maker and structure-breaker surfaces, respectively.^{7,8,15,16} It follows that structure-breaker ions adsorb more strongly on a structure-breaker surface and vice versa. It has been suggested that the silica surface is of structure-breaker type,^{8,18} but the precise structure of the silica–water interface is not known, and more importantly it varies with pH.¹⁶ The ion specific effects can be explained theoretically by including both the ion–surface hydration interaction and the ion–ion and ion–surface dispersion interactions.^{19,20} Recently, Parsons et al. showed that the experimentally observed adsorption sequence at the silica surface could be explained by using a modified Poisson–Boltzmann model that includes both the IIC and the hydration of the ions.²¹ It was also shown that the strongly hydrated ions retain their hydration shells while approaching the silica surface,²¹ a result that correlates well with the experimental results of Johnson et al.⁹ However, if these effects should oppose one another, the compatibility of the ion and surface water structures is more important than the ion polarizability for the specific adsorption, as was shown by López-León et al.⁷

Several techniques have been used to study the aggregation of colloidal silica including static and dynamic light scattering,^{22,23} viscosity and turbidity measurements,^{10,15,16} small-angle X-ray scattering,²⁴ and small-angle neutron scattering.²⁵ Recently, we have shown that the electrospray-scanning mobility particle sizer (ES-SMPS) technique can be used for kinetic evaluations of the aggregation behavior of silica dispersions; clear ion specific effects on the formation and disintegration of silica aggregates were observed.⁹ In a previous paper (Part I) we showed that the combination of the ES-SMPS method with synchrotron radiation small-angle X-ray scattering (SR-SAXS) could be used to monitor the initial aggregation of silica dispersions with various initial morphologies.¹ This combination facilitates the investigation of the early steps of the aggregate formation from the very first seconds of the reaction, which have thus far not been studied in detail. Here we aim to elucidate the effect of various electrolyte initiators on the stability of the gels formed from dispersions with various initial morphologies. To this end SR-SAXS and ES-SMPS measurements of the slow perikinetic aggregation, initiated by the addition of potassium chloride or potassium carbonate solutions, were performed. Potassium carbonate was included to investigate the anion effect on the aggregation and gel stability; moreover, to substitute NaCl for K₂CO₃ in applications

such as rock grouting^{26,27} or soil stabilization,²⁸ while maintaining the gel strength and permeability, is of interest for environmental reasons. The results were compared to those obtained in Part I for the aggregation of these dispersions in the presence of sodium chloride. To further explain the observed ion specificity, effective ion sizes were determined by fitting activity coefficients, calculated by MC simulations, to experimental data. A consistent model that describes resulting gel stability in relation to the aggregation initiators is proposed.

2. METHODS

2.1. Experimental Section. *Materials.* Stock solutions of the electrolytes (NaCl, KCl, and K₂CO₃, ~10% by weight) and the buffer-solution for the ES system (Ammonium acetate, 20 mM, pH 8.0) were prepared using water purified by a milli-Q purification system (18.2 MΩ cm, Synergy 185, Millipore). The sodium chloride (supra pure, Merck), potassium chloride (supra pure, Merck), potassium carbonate (pro analysi, Merck), ammonium acetate (pro analysi, Merck), and ammonia (pro analysi, Scharlau) were used as received. Three silica dispersions were included in this investigation, Sol 1, Sol 2, and two batches of Sol 3; all dispersions are commercially available products that were supplied by Eka Chemicals AB and used as received. Physical and chemical properties of the dispersions are listed in Supporting Information (SI, Table S1). From production the dispersions were stabilized with a small amount of Na₂O and contained no additional stabilizers, buffers, or surfactants.

Aggregation Experiments. As the methodology and experimental setups have previously been described in detail,^{1,9} only a short description will be given here. Slow aggregation of the silica dispersions (Sols 1, 2, 3 Dec, and 3 July) in the presence of NaCl (results shown in Part I), K₂CO₃, and KCl at constant temperature (20 °C) was monitored using ES-SMPS and SR-SAXS techniques. A gel time of about 40 min was achieved by adjusting the bulk electrolyte concentration in the reaction mixtures. This approach ensures that the gel formation kinetics, and most probably the gel structure, for a given dispersion are kept reasonably constant between the experiments.^{1,9} The gel structures formed from dispersions with various initial morphologies are not similar. However, as the gel time was kept constant, the gel networks had similar amount of time to evolve in the various mixtures. Therefore, this approach allows for comparative investigations of the aggregation kinetics of concentrated dispersions with diverse initial morphology. The point of gelation (PoG) was determined visually as the time at which the gel surface was stationary when the beaker containing the reaction mixture was turned upside down. To avoid local precipitation upon addition of the electrolyte solution, all experiments were performed with solutions of sufficiently low concentration added under thorough agitation. The weight percent SiO₂ and bulk electrolyte concentrations in the K₂CO₃ and KCl reaction mixtures as well as the obtained PoGs are listed in Table 1; when the concentrations were calculated, the volume of the particles was subtracted from the total volume. For the NaCl reaction mixtures this information is listed in Table S2 of the SI. To mimic the aggregation conditions used in applications such as rock grouting and soil stabilization, the pH of the reaction mixtures was not adjusted after electrolyte addition. This means that the pH of the chloride reaction mixtures decreased ~0.5–0.8 pH units, as compared to the pH of the pure dispersions, due to dilution. While, the pH of the carbonate

Table 2. Changes in Aggregate Mean Diameters and the Polydispersities during K_2CO_3 and KCl Initiated Aggregation as Monitored by ES-SMPS

electrolyte	K_2CO_3		KCl	
	mobility diameter (nm)	polydispersity part./agg.	mobility diameter (nm)	polydispersity part./agg.
sample				
Sol 1 _{initial}	27.8	0.19/-	27.6	0.20/-
Sol 1 _{500s}	39.7	0.20/0.24	34.2	0.19/0.28
Sol 1 _{1500s}	45.3	0.22/0.25	44.1	0.21/0.28
Sol 1 _{PoG}	50.8	0.23/0.25	50.5	0.22/0.28
Sol 1 _{final}	52.8	0.22/0.25	54.0	0.25/0.26
Sol 2 _{initial}	28.8	0.49/0.25	27.5	0.50/0.27
Sol 2 _{500s}	54.1	0.51/0.26	52.0	0.53/0.25
Sol 2 _{PoG}	63.9	0.63/0.27	62.2	0.32/0.35
Sol 2 _{final}	65.7	0.69/0.29	63.7	0.26/0.35
Sol 3 Dec _{initial}	20.9	0.40/0.22	20.2	0.41/0.21
Sol 3 Dec _{500s}	36.0	0.42/0.26	36.5	0.43/0.26
Sol 3 Dec _{PoG}	43.4	0.39/0.29	44.5	0.37/0.30
Sol 3 Dec _{final}	43.1	0.41/0.29	43.2	0.40/0.32
Sol 3 July _{initial}	20.1	0.37/0.26	19.8	0.41/0.24
Sol 3 July _{500s}	36.8	0.39/0.27	34.8	0.44/0.25
Sol 3 July _{PoG}	43.5	0.39/0.28	44.8	0.40/0.31
Sol 3 July _{final}	43.3	0.38/0.31	40.9	0.42/0.32

reaction mixtures increased ~ 0.2 – 0.3 pH units due to the high initial pH of the K_2CO_3 solution. The difference in pH between the chloride and carbonate mixtures was around 1 pH unit for Sols 1, 3 Dec, and 3 July, whereas it was 1.4 pH units for Sol 2. The SR-SAXS measurements were performed at the Austrian SAXS beamline at ELETTRA (Trieste, Italy).²⁹ The data were corrected for spatial distortion and electronic noise and then integrated to give $I(q)$, the scattered intensity as a function of the scattering angle q . Because of the limited beam time, the measurements were focused on the K_2CO_3 reaction mixtures; these experiments were then complemented with ES-SMPS measurements on both K_2CO_3 and KCl systems. The ES-SMPS measurements were performed at the University of Gothenburg; an ES unit (TSI Inc., ES model 3480) combined with a SMPS (TSI Inc., SMPS model 3936) were used to measure the size distribution of particles and aggregates during aggregation.

Morphology of the Pure Dispersions. The initial morphologies of the particles in these dispersions were evaluated in detail in Part I,¹ however, a short summary will be given here. Sol 1 consisted of monodisperse spherical particles, Sol 2 consisted of polydisperse spherical particles, and the Sol 3 batches contained preaggregates that were comprised of spherical primary particles with a diameter of 10–15 nm. The preaggregates displayed a range of nonspherical shapes from straight chains to more compact clusters. They were modeled as prolate ellipsoids; average equatorial and polar diameters of 16 and 38 nm, respectively, were obtained from scanning electron microscopy (SEM) images. It should be noted that the preaggregates were quite polydisperse and some of the structures showed polar diameters of 70–90 nm. The mean diameters of Sol 1 and 2, as measured from SEM images, were approximately 27 and 30 nm, respectively. The size distributions from the ES-SMPS measurements of the pure dispersions were fitted to a Gaussian or a log-Gaussian

distribution; the mean diameters and polydispersities obtained from the fitting are listed in Table S3 of the SI.

The hard sphere model has been shown to work well for systems comparable to the dispersions included in this investigation as well as for soft particles and clusters of soft particles.^{30–33} Therefore, the SR-SAXS data were fitted to the analytical expressions for the scattering arising from particles with a hard sphere interaction; for Sols 1 and 2 a spherical form factor was used, while an ellipsoidal form factor was used for Sol 3. Two parameters, that is, the particle diameter (D1) and the hard sphere diameter (HD), were obtained from the fitting of the hard sphere model (HS); when the ellipsoidal hard sphere model (EHS) was used, three parameters (D1, D2, and HD) were obtained. The HD represents the closest distance of approach between two particles in the dispersion. It incorporates the electrostatic interaction of particles, the gel layer surrounding the silica particles, and any possible hydration of the surface. The D1 values, in the case of Sol 3 D1 and D2 values, represent the dimensions of the scattering entity. The mean diameters and polydispersities of the pure dispersions obtained from the SR-SAXS analysis are listed in Table S4 of the SI.

2.2. Monte Carlo Simulations. Monte Carlo (MC) simulations were performed to calculate the activity coefficients of NaCl and K_2CO_3 salt solutions; the result of the calculations for the KCl system has been presented in a previous work.³⁴ The MC simulation method used in this study has been described in detail elsewhere;^{34,35} only the main features of this method will be summarized here. The MC simulations were performed by the standard Metropolis algorithm. A canonical ensemble was constructed by using a cubic box with periodic boundary conditions. The simulations were performed with the unrestricted primitive model (UPM) of the electrolytes. In the UPM model ions are considered as charged hard spheres of different sizes dissolved in the solvent, which is represented by the dielectric constant. To attain a certain electrolyte concentration in the cubic box, the side length was varied at a fixed total number of ions. The activity coefficients were determined by using a modified Widom particle insertion method in which the electroneutrality of cell is maintained by charge rescaling.³⁵ In the MC simulations reported here, large systems, that is, 1000 ions for 1:1 and 900 ions for 2:1 electrolytes, are used. Long simulations, that is, chains of 95 million MC configurations, were generated to obtain the activity coefficients. The calculated activity coefficients were fitted to the experimental data by adjusting ion radii. In this way we obtained the best fitted ion radii which describe the experimentally determined activity coefficients in a given concentration range. In the case of NaCl and KCl the chloride radius was fixed to the crystallographic value (0.181 nm), and the cation radius was adjusted to obtain best fit to the experimental data. For the K_2CO_3 salt the potassium radius was fixed to the crystallographic size (0.134 nm), while the CO_3^{2-} radius was adjusted.

3. RESULTS AND DISCUSSION

3.1. Silica Aggregation in the Presence of Various Electrolytes. *Aggregate Sizes and Gel Morphology.* The aggregation of the three dispersions in the presence of K_2CO_3 and KCl was monitored with ES-SMPS, and the obtained size distributions were normalized according to the procedure described in Johnson et al.⁹ Bimodal size distributions were obtained for all reaction mixtures, which indicates that detachable aggregates and primary particles were present in the gel structure well past the PoG.^{1,9} In

this context detachable refers to the ability of particles and aggregates to separate from the 3D gel network. The size distributions of the aggregating reaction mixtures of Sol 1 were fitted to a sum of two Gaussians, and the size distributions obtained during the aggregation of Sols 2 and 3 were fitted to a sum of a Gaussian and a log Gaussian. The mean diameters and polydispersities of the aggregates obtained from the fitting for selected points during the aggregation are listed in Table 2 (extended in Table S5 of the SI). For comparison, the aggregate diameters and polydispersities for the aggregation of these dispersions in the presence of NaCl are listed in Table S6 of the SI. For a given dispersion, the aggregates formed in the presence of various electrolytes were of similar sizes, and only small differences could be distinguished. For example, the Sol1/ K_2CO_3 mixture displayed slightly larger mean aggregate diameters at the intermediate stage of the aggregation process. The largest aggregates in the solid gels of Sol 2 were observed in the NaCl mixture, while the smaller aggregates were formed in the presence of KCl. The Sol3/NaCl reaction mixtures showed the smallest gel aggregates. Also, the effect of aging of Sol 3 could be distinguished as K_2CO_3 and KCl displayed equally large aggregates in the gel samples of Sol 3 Dec, whereas the July batch showed larger aggregates in the K_2CO_3 gels.

In this investigation the bulk electrolyte concentrations were adjusted to attain a gelation time of ~ 40 min, and the required bulk electrolyte concentration reflects the screening efficiency of the counterions (concentrations listed in Table 1 and Table S2 of the SI). A lower bulk concentration corresponds to more strongly adsorbed ions at the particle surface and thus a higher screening efficiency.⁹ It can be seen that for each electrolyte the polydisperse spherical particles (Sol 2) required the highest concentration to screen the total surface. This can partly be a particle size effect as it has recently been shown that screening of charged small particles is considerably enhanced compared to the larger particles.³⁶ Sol 2 contained a considerable amount of particles larger than 30 nm, and these particles will be screened less effectively by the counterions. Therefore, a higher electrolyte concentration was required to reach the PoG as compared to, for instance, Sol 1. All investigated dispersions were most efficiently screened in the KCl mixtures compared to the NaCl mixtures. These results are in agreement with the previously obtained adsorption sequence of alkali ions at the silica surface.^{9,10,15,16} The K_2CO_3 bulk concentrations required to sufficiently screen a specific dispersion were approximately equal to the required NaCl concentrations for that same dispersion. The higher pH in the K_2CO_3 reaction mixtures leads to an increased surface charge which, in combination with the lower activity of the potassium ions in the potassium carbonate solution, explains the concentration differences between the KCl and K_2CO_3 reaction mixtures.

The aggregate mean diameters obtained from the ES-SMPS measurements were used to calculate the mean aggregate volumes. To visualize the ion-specific effects of the electrolytes, the obtained aggregate volumes were corrected for the bulk electrolyte concentration and the weight percent SiO_2 in the reaction mixtures (Table 1 and Table S2 of the SI). The increase in corrected aggregate volume as the aggregation proceeded is shown in Figure S1 of the SI. The largest aggregate volumes were formed in the potassium chloride reaction mixture of each dispersion, and the aggregate volumes of the K_2CO_3 reaction mixtures were generally smaller compared to the other electrolytes. Straight lines were fitted to the initial increase of the corrected aggregate volumes; thus, initial aggregation rates were obtained.

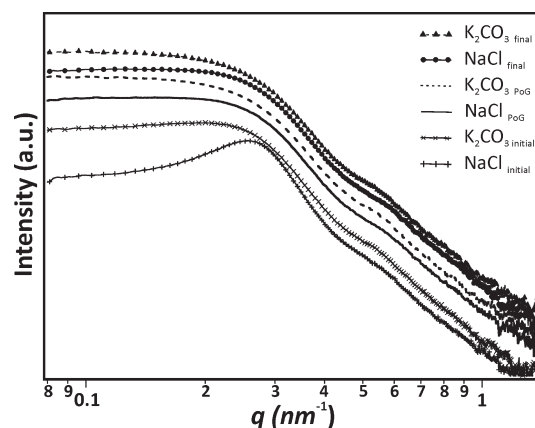


Figure 1. $I(q)$ vs q for the aggregation of Sol 1 initiated with NaCl and K_2CO_3 . The aggregation was monitored in the stopped-flow cell with a CCD camera.

The trend observed in Johnson et al.⁹ with a higher initial rate in the presence of KCl, as compared to NaCl, was found for all dispersions included in this investigation. The addition of K_2CO_3 seemingly resulted in the lowest aggregation rate for almost all dispersions; the exception was Sol 1 where the K_2CO_3 and NaCl aggregation rates were equal. However, this is a result of the higher surface charge in these mixtures which requires higher electrolyte concentrations to be sufficiently screened. The aging of Sol 3 led to a decrease in the aggregation rate for NaCl and K_2CO_3 and an increase in the aggregation rate for KCl. The aggregation rate decreases as a result of an increase in the gel layer due to Oswald ripening.² Possibly, the change of the surface due to aging increases the structure-breaker character of the surface, which leads to the observed increase in the aggregation rate for KCl.

The aggregation of the three dispersions in the presence of K_2CO_3 was also monitored by SR-SAXS. The sequence of $I(q)$ versus q plots for the aggregation of Sol 1 in the presence of NaCl and K_2CO_3 is shown in Figure 1. For clarity, each curve is shifted vertically, and only the initial, PoG, and final measurements are plotted. The $I(q)$ curve for the pure Sol 1 was dominated by the structure factor contribution that arise from the interparticle interactions; the structure peak showed a maximum intensity at $q = 0.257 \text{ nm}^{-1}$. A weak second order of the main $S(q)$ peak, which can be related to the packing of the primary particles in the solution,¹ was also observed as a small hump in the $I(q)$ curve around $q = 0.5 \text{ nm}^{-1}$. It can be seen that the structure peak was obscured by the increasing intensity at lower q ($q < 0.2 \text{ nm}^{-1}$) at an earlier stage for the aggregation initiated by the addition of K_2CO_3 as compared to NaCl. Close to the PoG the scattering curves obtained with the two electrolytes were similar. For instance, the second order $S(q)$ hump was also present in the gel sample of Sol1/ K_2CO_3 , which indicates that unaggregated primary particles were still present in the sample after the PoG.¹ The change of the scattering curves, during aggregation and after the PoG, for Sol2/ K_2CO_3 and Sol3/ K_2CO_3 was also similar to that observed for the NaCl mixtures. Thus, comparable gel morphologies were obtained with the two electrolytes. The parameters obtained from the fitting of the SR-SAXS data sets acquired for each sol at selected points after the K_2CO_3 addition are presented in Table 3 (extended in Table S7 of the SI). For comparison, the aggregate diameters and polydispersities of these dispersions in the presence of NaCl are listed in Table S6 of the SI.

Table 3. Changes in Aggregate Mean Diameters and Polydispersities during K_2CO_3 Initiated Aggregation as Monitored by SR-SAXS^a

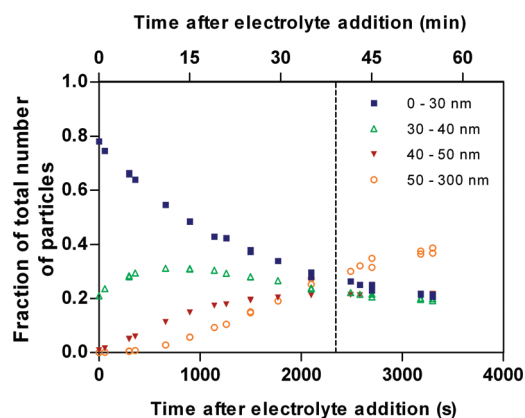
sample	D1/D2 (nm)	polydispersity	hard diameter (nm)
Sol 1 _{initial}	15.5	0.16	24.4
Sol 1 _{500s}	15.4/31.2	n/a	24.3
Sol 1 _{1500s}	15.4/38.3	n/a	24.3
Sol 1 _{PoG}	50.4	0.16	24.4
Sol 1 _{final}	50.4	0.16	24.4
Sol 2 _{initial}	21.6	0.40	26.5
Sol 2 _{500s}	51.2	0.28	28.4
Sol 2 _{PoG}	58.8	0.22	29.5
Sol 2 _{final}	60.3	0.22	30.8
Sol 3 Dec _{initial}	5.6/49.2	n/a	8.6
Sol 3 Dec _{500s}	5.6/86.3	n/a	10.1
Sol 3 Dec _{PoG}	5.6/108.6	n/a	10.9
Sol 3Dec _{final}	5.6/109.8	n/a	13.2

^a The data were fitted to the scattering arising from spherical (Sol 1 and 2) or ellipsoidal (Sol 3) particles with hard sphere interaction.

The initial changes in the scattering patterns of the Sol1/NaCl and Sol1/ K_2CO_3 mixtures could indicate that the early aggregation was somewhat faster in the K_2CO_3 mixture. However, the fitting showed that the obtained aggregate sizes in a specific dispersion were almost independent of aggregation initiator. Thus, similar aggregate sizes and gel morphologies were attained in the various mixtures of a given dispersion as indicated by the aggregate diameters obtained from the ES-SMPS and SR-SAXS measurements as well as the obtained scattering patterns of the unperturbed gels.

Aggregate Formation. The size range analyzed with ES-SMPS (7–300 nm) was divided into four size intervals (7–30 nm, 30–40 nm, 40–50 nm, and 50–300 nm), and the fraction of total number of particles (FTP) in these size intervals was calculated. These size intervals were chosen as such because the Sol1/NaCl mixture showed a clear sequential increase in these size ranges.¹ The variation of the FTP for the Sol1/ K_2CO_3 is shown in Figure 2. The corresponding results obtained for Sols 2 and 3 with K_2CO_3 are shown in Figure S2 and for all dispersions in the presence of KCl in Figure S3 of the SI. For comparison the variation of the FTP for these dispersions in the presence of NaCl is shown in Figure S4 of the SI. The 7–30 nm size interval (and 30–40 nm in the case of Sol 2) corresponds to the primary particles, or preaggregates in the case of Sol 3, in the pure dispersions, and it can be seen that all gel samples contained detachable primary particles well past the PoG. The aggregation behavior in the presence of K_2CO_3 and KCl was very similar to that observed in the presence of NaCl for all dispersions investigated.

In a previous paper (Part I) it was shown that the structure of the formed aggregates can be deduced from the change of the FTP in the four size intervals during aggregation.¹ Initially, Sol 1 showed an increase in the size range 30–40 nm, and this increase peaked around 500 s simultaneously as the 40–50 nm range started to increase; at about 1000 s the range 50–300 nm began to increase linearly. This is consistent with an aggregation that starts with the formation of dimers, followed by the formation of trimers; subsequently, the dimers and trimers form larger spherical aggregates containing 4 to 5 primary particles.¹ Sol 2 formed

**Figure 2.** Change in the fraction of total number of particles during aggregation of Sol 1 initiated with K_2CO_3 . A dashed vertical line indicates the point of gelation.

large aggregates in the initial stages of the aggregation, as indicated by the immediate increase in the 50–300 nm size range upon electrolyte addition. Throughout the aggregation and past the addition of smaller particles. During the aggregation of Sol 3, only a small increase of the FTP in the size ranges 40–50 and 50–300 nm was seen, and the detachment of aggregates (size range 50–300 nm) from the 3D gel structure of the Sol 3 gels was almost negligible. At the PoG the FTP in the size interval 7–30 nm started to increase, while the FTP in the other intervals started to decrease. This indicates that a very stable gel structure was formed in these dispersions, and it was concluded in Part I that the preaggregated particles preferably joined end-to-end so that the produced aggregates displayed an open, more elongated morphology.¹ The analysis of the changes in FTP during aggregation indicates that the aggregate formation in a specific dispersion was independent of the aggregation initiator.

3.2. Effects of Ion Specificity on Gel Stability. *Rate of the Stability Increase.* As the aggregation proceeds, the stability of the aggregates increases; at the PoG the aggregates form a network that spans the entire volume, and the stability of the 3D gel network starts to increase. When the stability of the network increases, the amount of detachable particles and aggregates in the detectable size range decreases.¹ The gel stability increase was determined by monitoring the change in total aerosol mass (Figure 3). It can be seen that the total aerosol particle mass decreased drastically around the PoG, which corresponds to a rapid decrease in the amount of detachable particles and aggregates. The general stability of the gels increased in the following order: Sol 1 < Sol 2 < Sol 3 Dec \approx Sol 3 July, as indicated by the relative drop-off in aerosol mass. Moreover, the start of the drop-off in aerosol mass, in relation to the exact PoG, gives an indication of the rate of the strength increase; an early drop-off suggests a faster strength increase in the formed 3D gel structure. The points where the decrease started in the various dispersion/electrolyte mixtures are indicated by arrows (Figure 3). The decrease in aerosol mass started prior to, or at, the PoG for all reaction mixtures containing sodium chloride, whereas the decrease started after the PoG for all mixtures containing potassium ions. Furthermore, a clear difference between the potassium salts could be seen for Sols 1 and 2. The decrease was much less pronounced and occurred well past the PoG in the K_2CO_3 mixtures as compared to the KCl mixtures; for example, in Figure 3a the decrease had

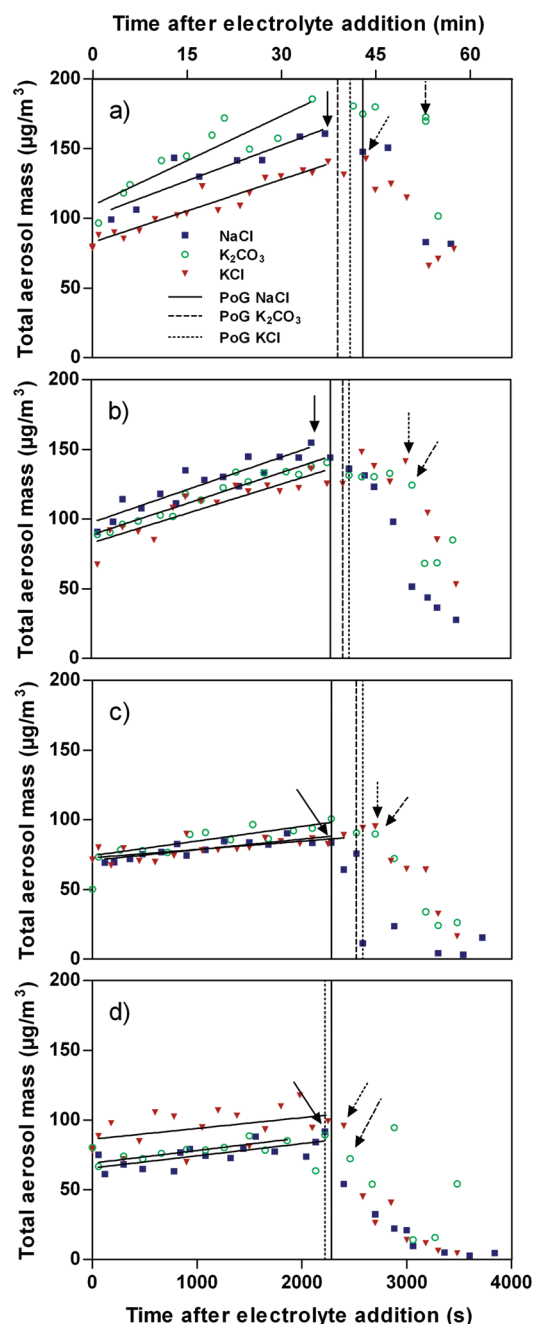


Figure 3. Change in total aerosol mass during aggregation of (a) Sol 1, (b) Sol 2, (c) Sol 3Dec, and (d) Sol 3 July in the presence of \blacksquare , NaCl; \circ , K_2CO_3 , and \blacktriangledown , KCl. Vertical lines indicate the points of gelation: NaCl (solid), K_2CO_3 (dashed), and KCl (dotted).

only just started when measurements were terminated some 20 min past the PoG.

The difference between the three electrolytes, and especially the potassium salts, was not as prominent for the Sol 3 gels (Figure 3c,d). However, the increased gel stability of Sol 3 could also be observed as a decrease of the FTP in the size range 50–300 nm coupled with an increase of the FTP in the 7–30 nm size range and as a decrease of the aggregate volume.¹ The decrease of the FTP in the aggregate size range (50–300 nm) was not as prominent in the mixtures containing potassium ions (Figures S2 and S3 of the SI). Furthermore, the increase in the small size

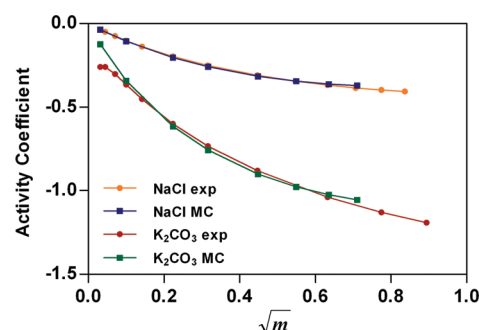


Figure 4. Calculated values of the mean activity coefficients of the NaCl and K_2CO_3 electrolyte solutions. The best fit radii obtained from the MC calculations: $\text{Na}^+ = 0.180$ nm, $\text{K}^+ = 0.134$ nm, $\text{Cl}^- = 0.181$ nm, and $\text{CO}_3^{2-} = 0.253$ nm. The calculated values are compared with the experimentally determined mean activity coefficients as taken from refs 37 and 38 for NaCl and K_2CO_3 , respectively.

range (7–30 nm) occurred at a later stage in the KCl mixtures as compared to NaCl; for the K_2CO_3 reaction mixtures this increase was almost insignificant. Finally, the aggregate volume decrease was smaller for the KCl reaction mixtures as compared to the NaCl mixtures, while the aggregate volume remained constant after the PoG in the K_2CO_3 mixtures (Figure S1 of the SI). Overall, the obtained results indicate that the development of a strong 3D gel structure in the Sol 3 batches followed the same general trends as Sols 1 and 2. Thus, the rate of the stability increase of the gel structures increased in the following order $\text{K}_2\text{CO}_3 < \text{KCl} < \text{NaCl}$. The observed differences cannot be due to structural variations in the gels because each specific dispersion displayed similar aggregate growth, which rendered comparable gel structures, in the presence of the various electrolytes, see Section 3.1. Thus, these effects must be due to ion-specific interactions between the aggregates that form the 3D gel structures.

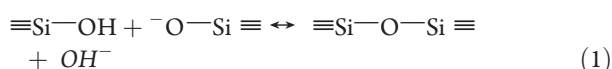
Hydration Structure of the Ions. To classify the water structure of the ions, the calculated mean ionic activity coefficients of K_2CO_3 and NaCl were compared with the corresponding experimental data;^{37,38} see Figure 4. The ionic radii used in the MC simulations were 0.168 and 0.181 nm for Na^+ and Cl^- , respectively. The CO_3^{2-} ion was considered as hydrated, and the ionic radii was optimized to 0.24 nm. A good agreement between the calculated and experimental data was found up to a concentration of 0.6 M. We have previously shown that the activity coefficients of KCl can be fitted up to 0.8 M by assigning the ionic radii 0.134 and 0.181 nm for K^+ and Cl^- ions, respectively.³⁴ The difference between the crystallographic and optimized hydrated radius can be used to calculate the hydration number of the ions, and the hydration numbers of K^+ and Cl^- in the KCl solution are 0 for both ions.³⁴ Whereas the calculated hydration numbers of Na^+ and Cl^- are 1.4 and 0, respectively. The optimized hydrated radius of CO_3^{2-} is larger than its crystallographic radius (0.178 nm), and the calculated hydration number of the carbonate ion in the K_2CO_3 solution was ~ 3 .

Hence, the preformed MC calculations indicate that the Na^+ and CO_3^{2-} ions are strongly hydrated, which suggest that they have a structure-maker character. In a recent review Marcus have also classified the CO_3^{2-} ion as a structure maker, whereas K^+ and Cl^- were classified as structure-breaker ions.¹⁷ The Na^+ ion was classified as an intermediate ion, displaying both structure-maker and structure-breaker characteristics.¹⁷ Note that these classifications are based on the extensive review of results obtained

by a number of different experimental techniques along with computer simulations. The obtained hydration numbers are in good agreement with the irrotationally bound water molecules found by the dielectric spectroscopy.¹⁷ However, in the case of Na^+ the dielectric spectroscopy shows that 2–3 irrotationally bound water molecules, compared to 1.4 water molecules which was obtained from the MC simulations. This difference is understandable because in the MC simulations ions are considered as charged hard spheres dissolved in a dielectric continuum. Properties of real salt solutions, such as the decrease in the dielectric constant, the molecular nature of the solvent, and the overlap of hydration layers at increasing ion concentrations, are not included in this simple model. To obtain a better fit to the experimental data these effects are compensated for by adjusting the ion radii. Thus, fitting the experimental data to high concentrations, where the hydration layer overlap is significant, will result in small values of fitted ionic radii and consequently low hydration numbers.

Overall, these results are in accordance with the prevailing understanding of ion hydration, that is, small ions with high charge density bind water molecules more strongly than large weakly charged ions. This tight binding of water molecules around small ions leads to a larger hydrated ion radii. Due to the interaction with the ion, the water molecules in the hydration layer of strongly hydrated ions can become polarized.^{39,40} This causes the bond length of one of the O–H bonds to increase, which in turn makes the hydrogen more acidic, and a local acidic environment is formed around strongly hydrated ions.^{39,40}

Effect of Ion Hydration on Siloxane Bond Formation. Silica has a low Hamaker constant, which can be further decreased by electrolyte addition,⁴¹ and as a result weak van der Waals interactions.^{2,42} Therefore, it has been postulated that the aggregates are not primarily stabilized by van der Waals interactions, rather the particles aggregate irreversibly upon contact due to the formation of covalent bonds according to reaction 1.⁴²



Nevertheless, it has been shown that the silica aggregation, at least initially, is fully reversible,^{9,42} and the structure of the formed aggregates indicate that they broke apart and reformed many times prior to the PoG.^{1,23,43} This behavior can be explained by the fact that energy required to break the Si–O bond is approximately half of the bond strength.⁴⁴ Thus, the silica surface is a highly dynamic surface, and siloxane bonds at the surface and in the gel layer constantly break and reform.⁴⁵ When the particles come into contact siloxane bonds can start to form, and the aggregate stability increases as the number of covalent bonds between the particles increase. However, owing to the fact that the bonds can break and reform, this process is slow. Moreover, the contribution of the covalent bonds to the stability of the aggregates will fluctuate during the aggregation. Hence, it is possible that the particle and aggregate intercollisions can result in aggregate disintegration while the system is mobile.

We have recently shown that the more polarizable alkali ions produced the most stable aggregates and the increased stability could be attributed to the IIC interaction.⁹ In addition, the effect of the strongly hydrated ions on the aggregate internal osmotic pressure could be observed; the more strongly hydrated ions adsorb at a distance further away from the surface and can exert a higher osmotic pressure due to their hydration layer. The

increased osmotic pressure, in combination with the lower IIC interaction of these ions, made these aggregates less stable.⁹ Thus, aggregates with a stronger internal repulsion tend to be less stable, whereas aggregates with additional internal attractions are on average more stable. As the aggregation progress and the number of interparticle bonds increase, more aggregates become stable; that is, they cannot be broken apart by the collisions. Once a sufficient amount of stable aggregates have formed, a network that spans the entire volume develops, and the system becomes arrested.

It seems intuitive that more stable aggregates should lead to a more stable gel, and this has indeed been the case in many investigations.^{10,15,16} However, the opposite behavior with respect to gel stability has also been reported in the literature⁴⁶ and was observed in this investigation. As long as the system is mobile, the intercollisions cause the less stable aggregates to break apart more often (on average). However, the local acidic environment provided by the strongly hydrated ions can catalyze the formation of covalent siloxane bonds by stabilizing the hydroxyl leaving group in reaction 1.⁴² This is in agreement with the ion-specific effects observed for the polymerization rate of silica.⁴⁷ We propose that once the system is arrested the effect of the strongly hydrated ions on the rate of bond formation becomes noticeable, and therefore, the more pronounced gel stability increase is observed in the presence of more strongly hydrated ions, even though the more polarizable ions form the most stable aggregates.⁹ The lower rate of stability increase in the K_2CO_3 gels is due to the higher concentration of hydroxyl ions in these gels, which according to reaction 1 increases the rate of siloxane bond breakage. The ion-specific effects before and after system arrest are depicted schematically in Figure 5. The ions and silica particles are not to scale, and features are exaggerated for clarity. The suggested mechanism can possibly explain some of the contradicting results previously obtained for silica systems.^{10,15,16,46}

Distribution of Ions at the Surface. The aerosol mass started to increase after electrolyte addition; this increase is due to the density difference between the primary particles and the aggregates (Figure 3). The mass calculations were performed with the assumption that all aerosol particles were of bulk density, but as the aggregates grow they become fractal. Therefore, the density of the aggregates is lower compared to the primary particles, and the aerosol mass appears to increase prior to the PoG. A lower increase of the aerosol mass during aggregation corresponds to a more compact aggregate structure. It can be seen that the Sols 1 and 2 formed more compact aggregates in the presence of KCl, as compared to the mixtures containing NaCl or K_2CO_3 . The increase of the total aerosol mass during aggregation was less pronounced for Sol 3, which suggests that the density of the formed aggregates was close to the density of the preaggregates. In addition, Sol 3 formed equally dense aggregates in the presence of the various electrolytes. The observed variation in aggregate density could be due to differences in the distribution of ions near the silica surface. The silica surface is most often classified as a structure-breaker surface,^{8,16} and owing to the water structure of the strongly hydrated Na^+ and CO_3^{2-} ions they will adsorb further from the silica surface compared to less hydrated ions such as K^+ and Cl^- .^{16,21} We propose that the Na^+ and CO_3^{2-} ions form less compact aggregates because these ions require a larger space within the aggregates. The fact that the Cl^- ions adsorb closer to the silica surface, even though the CO_3^{2-} ions are larger and more polarizable is in accordance with the results of López-Léon et al.⁷

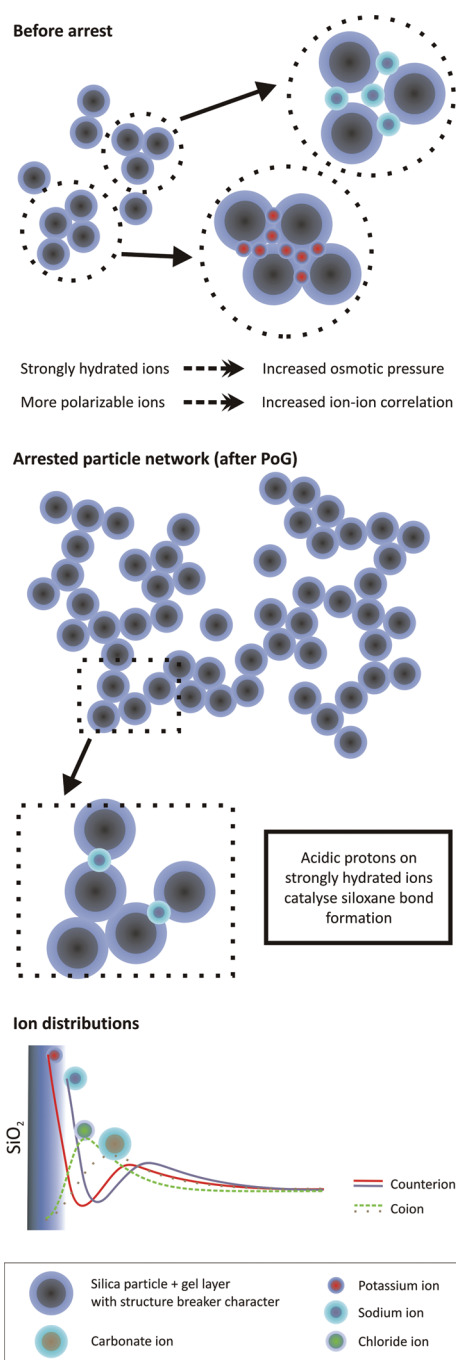


Figure 5. Schematic illustrations of the proposed ion-specific effects that influence the interaction between colloidal silica particles before and after system arrest (top) and the ion distributions that could result from these interactions (bottom). The ion distributions as well as the ion and particle sizes are not to scale, and the features are exaggerated for clarity.

Furthermore, the extension of the gel layer can be obtained from the difference between the diameter of the particle core (D1) and the hard sphere diameter (HD).¹ Upon electrolyte addition the charges within the gel layer are screened, and the layer deflates.^{1,48} For all dispersions investigated the contraction of the gel layer was less pronounced in the presence of K₂CO₃ compared to NaCl. The slight pH increase leads to a higher surface charge in the K₂CO₃ mixtures. However, the surfaces were screened to the same extent, since the same PoGs were

obtained; therefore, it is reasonable to assume that the gel layer contraction in the NaCl and K₂CO₃ reaction mixtures should be similar. The fact that the addition of K₂CO₃ rendered a somewhat more inflated the gel layer also suggests that the CO₃²⁻ ions adsorbed further from the surface. Due to a limited beam time, no SR-SAXS measurements were performed for the KCl reaction mixtures, and the gel layer contraction can therefore not be evaluated for these systems. To conclude, the more strongly hydrated ions (Na⁺ and CO₃²⁻) form less compact aggregates because these ions require a larger space within the aggregates. A suggestion for the ion distributions near the silica surface, based on the results obtained in this investigation, is schematically depicted in Figure 5.

4. CONCLUSION

The ion specific effect of sodium chloride, potassium chloride, and potassium carbonate on the aggregation of three silica dispersions was investigated using ES-SMPS and SR-SAXS techniques. The results showed that the diameters of the aggregates, the aggregate formation, and the obtained gel morphologies for a given dispersion were similar or equal irrespective of the added electrolyte. However, the rate of the gel stability increase was dependent on the aggregation initiator used. For all dispersions the rate increased in the following order K₂CO₃ < KCl < NaCl. The observed differences cannot be due to structural variations in the gels because each specific dispersion formed comparable gel structures in the presence of the various electrolyte.

It has been previously shown that structure-breaker ions such as K⁺ form the most stable aggregates due to a higher IIC interaction.⁹ Even so, the rate of the gel strength development was faster in the presence of the structure-maker ions such as Na⁺. The structure-maker ions can polarize the water molecules in the hydration layer so that the layer becomes more acidic and the local acidic environment facilitate the formation of siloxane bonds. Owing to the fact that the hydration layers of the structure-maker ions also lead to an increased osmotic pressure in the aggregates, this effect is masked prior to gel formation. The low rate of the stability increase in the presence of K₂CO₃ is due to the higher concentration of hydroxyl ions, which inhibits the formation of covalent bonds. For silica particles with a more reactive surface the catalyzing effect of the Na⁺ ions was not as important, and the correlation between the rate of the gel stability increase and the electrolyte initiator was therefore less pronounced.

■ ASSOCIATED CONTENT

S Supporting Information. Physical and chemical properties of the pure dispersions (Table S1). Silica and electrolyte concentrations in NaCl reaction mixtures (Table S2). Mean diameters and polydispersities of the pure dispersions obtained with ES-SMPS and SR-SAXS (Tables S3 and S4). Change in mean diameters and polydispersities during aggregation (Tables S5, S6, and S7). Increase in mean aggregate volume during the aggregation (Figure S1). Change in fraction of total number of particles for K₂CO₃ and KCl reaction mixtures (Figures S2 and S3). Change in fraction of total number of particles for NaCl reaction mixtures (Figure S4). This material is available free of charge via the Internet at <http://pubs.acs.org>.

AUTHOR INFORMATION

Corresponding Author

*E-mail: ann-catrin.johnson@chem.gu.se.

ACKNOWLEDGMENT

The authors thank Dr. Ann Terry and Dr. Richard Heenan for scientific insights and valuable help with fitting the data using FISH, Dr. Heinz Amenitsch and the Elettra staff for their help with the SR-SAXS measurements, Inger Jansson at Eka Chemicals for fruitful discussions, and Dr. Staffan Johansson for valuable comments on the manuscript. Further, the authors thank Jenny Lindvall and Catarina Petersen for valuable laboratory assistance.

REFERENCES

- (1) Johnson, A.-C. J. H.; Camerani, M. C.; Abbas, Z. *J. Phys. Chem. B* **2011**, *115*, 765.
- (2) Iler, R. K. *The Chemistry of Silica*; Wiley Interscience: New York, 1979.
- (3) Bergna, H. E. *The Colloid Chemistry of Silica*; American Chemical Society: Washington, DC, 1994.
- (4) Hunter, R. J. *Foundations of Colloid Science*; Oxford University Press, Inc.: New York, 2001.
- (5) Boström, M.; Deniz, V.; Franks, G. V.; Ninham, B. W. *Adv. Colloid Interface Sci.* **2006**, *123–126*, 5.
- (6) Lyklema, J. *Chem. Phys. Lett.* **2009**, *467*, 217.
- (7) López-León, T.; Santander-Ortega, M. J.; Ortega-Vinuesa, J. L.; Bastos-González, D. *J. Phys. Chem. C* **2008**, *112*, 16060.
- (8) Dumont, F.; Warlus, J.; Watillon, A. *J. Colloid Interface Sci.* **1990**, *138*, 543.
- (9) Johnson, A.-C. J. H.; Greenwood, P.; Hagström, M.; Abbas, Z.; Wall, S. *Langmuir* **2008**, *24*, 12798.
- (10) Franks, G. V. *J. Colloid Interface Sci.* **2002**, *249*, 44.
- (11) Lyklema, J. *Adv. Colloid Interface Sci.* **2003**, *100–102*, 1.
- (12) Attard, P. *Phys. Rev. E* **1993**, *48*, 3604.
- (13) Kjellander, R. *Ber. Bunsenges. Phys. Chem.* **1996**, *100*, 894.
- (14) Greberg, H.; Kjellander, R. *J. Chem. Phys.* **1998**, *108*, 2940.
- (15) Trompette, J. L.; Meireles, M. J. *Colloid Interface Sci.* **2003**, *263*, 522.
- (16) Trompette, J. L.; Clifton, M. J. *J. Colloid Interface Sci.* **2004**, *276*, 475.
- (17) Marcus, Y. *Biophys. Chem.* **1994**, *51*, 111.
- (18) Manciu, M.; Calvo, O.; Ruckenstein, E. *Adv. Colloid Interface Sci.* **2006**, *127*, 29.
- (19) Ninham, B. W.; Yaminsky, V. *Langmuir* **1997**, *13*, 2097.
- (20) Tavares, F. W.; Bratko, H. W.; Blanch, H. W.; Prausnitz, J. M. *J. Phys. Chem. B* **2004**, *108*, 9228.
- (21) Parsons, D. F.; Boström, M.; Maceina, T. J.; Salis, A.; Ninham, B. W. *Langmuir* **2010**, *26*, 3323.
- (22) Kobayashi, M.; Juillerat, F.; Galletto, P.; Bowen, P.; Borkovec, M. *Langmuir* **2005**, *21*, 5761.
- (23) Tourbin, M.; Frances, C. *Chem. Eng. Sci.* **2008**, *63*, 5239.
- (24) Schantz Zackrisson, A.; Skov Pedersen, J.; Bergholtz, J. *Colloids Surf., A* **2008**, *315*, 23.
- (25) Muzny, C. D.; Straty, G. C.; Hanley, H. J. M. *Phys. Rev. E* **1994**, *50*, 675.
- (26) Funehag, J.; Gustafson, G. *Tunnelling Underground Space Technol.* **2008**, *23*, 1.
- (27) Funehag, J.; Gustafson, G. *Tunnelling Underground Space Technol.* **2008**, *23*, 9.
- (28) Gallagher, P. M.; Lin, Y. J. *Geotech. Geoenviron. Eng.* **2009**, *135*, 1702.
- (29) Amenitsch, H.; Rappolt, M.; Kriechbaum, M.; Mio, H.; Laggner, P.; Bernstorff, S. *J. Synchrotron Radiat.* **1998**, *5*, 506.
- (30) Qiu, D.; Cosgrove, T.; Howe, A. M.; Dreiss, C. A. *Langmuir* **2006**, *22*, 546.
- (31) Gomme, C.; Blacher, S.; Goderis, B.; Pirard, R.; Heinrichs, B.; Alié, C.; Pirard, J.-P. *J. Phys. Chem. B* **2004**, *108*, 8983.
- (32) Stieger, M.; Skov Pedersen, J.; Lindner, P.; Richtering, W. *Langmuir* **2004**, *20*, 7283.
- (33) Posselt, D.; Skov Pedersen, J.; Mortensen, K. *J. Non-Cryst. Solids* **1992**, *145*, 128.
- (34) Abbas, Z.; Ahlberg, E.; Nordholm, S. *J. Phys. Chem. B* **2009**, *113*, 5905.
- (35) Svensson, B. R.; Woodward, C. E. *Mol. Phys.* **1988**, *64*, 247.
- (36) Abbas, Z.; Labbez, C.; Ahlberg, E.; Nordholm, S. *J. Phys. Chem. C* **2008**, *112*, 5715.
- (37) Hamer, W. J.; Wu, Y.-C. *J. Phys. Chem. Ref. Data* **1972**, *1*, 1047.
- (38) Roy, R. N.; Gibbons, J. J.; Williams, R.; Godwin, L.; Baker, G.; Simonson, J. M.; Pitzer, K. S. *J. Chem. Thermodyn.* **1984**, *16*, 303.
- (39) Depasse, J. *J. Colloid Interface Sci.* **1999**, *220*, 174.
- (40) Bernasconi, L.; Baerends, E. J.; Sprik, M. *J. Phys. Chem. B* **2006**, *110*, 11444.
- (41) Depasse, J. *J. Colloid Interface Sci.* **1997**, *188*, 229.
- (42) Depasse, J.; Watillon, A. *J. Colloid Interface Sci.* **1970**, *33*, 430.
- (43) Yates, P. D.; Franks, G. V.; Jameson, G. J. *Colloids Surf., A* **2008**, *326*, 83.
- (44) McPherson, J. W. *J. Appl. Phys.* **2006**, *99*, 083501.
- (45) Yaminsky, V. V.; Ninham, B. W.; Pashley, R. M. *Langmuir* **1998**, *14*, 3223.
- (46) Colic, M.; Fisher, M. L.; Franks, G. V. *Langmuir* **1998**, *14*, 6107.
- (47) Gorrepati, E. A.; Wongthahan, P.; Raha, S.; Fogler, H. S. *Langmuir* **2010**, *26*, 10467.
- (48) Vigil, G.; Xu, Z.; Steinberg, S.; Israelachvili, J. *J. Colloid Interface Sci.* **1994**, *165*, 367.